

Millimetric Properties of IRAS Galaxies (III): Luminosity Functions and Contributions to the Sub-Mm Sky Background

Alberto Franceschini⁽¹⁾, Paola Andreani⁽¹⁾ and Luigi Danese⁽²⁾

⁽¹⁾ *Dipartimento di Astronomia di Padova, vicolo dell'Osservatorio 5, I-35122 Padova, Italy.*

e-mail: franceschini@astrpd.pd.astro.it

⁽²⁾ *Scuola Internazionale Superiore di Studi Avanzati – Trieste –IT*

Submitted to MNRAS: August 1996

ABSTRACT

We exploit observations at 1.25 mm with the ESO-SEST telescope of a southern galaxy sample, selected from the IRAS PSC and complete to $S_{60} = 2 Jy$, to derive the FIR and mm luminosity functions and the conditional probability distributions of FIR and mm luminosity of galaxies. The reliability of these estimates is ensured by the good observed correlation of the far-infrared and mm emissions. This detailed knowledge of the millimetric properties of galaxies is used to simulate the extragalactic sub-mm sky (background intensity, small-scale anisotropy signals, and discrete source statistics) – that will be investigated soon by a variety of ground-based and space observatories. We find, in particular, that the recent tentative detection of a sub-mm background would require, if confirmed, strong evolution with cosmic time of the galaxy long-wavelength emissivity. We finally emphasize the difficulty to test such evolution through observations from currently available millimetric sites on ground.

Key words: cosmic microwave background - cosmology : observations - diffuse radiation - infrared: ISM: continuum

1 INTRODUCTION

Observations in the largely unexplored spectral domain between $100\mu m$ and $1300\mu m$ are expected to provide a new important channel for the investigation of the high-redshift universe and the exploration of the 'dark ages' after decoupling, for obvious reasons related to the effect of redshift – bringing optical-UV photons to longer wavelengths – and of dust – degrading the emitted light to even lower energies.

The detection of high- z galaxies at these wavelengths is emphasized by the relative faintness of the local source populations, and by the strong and positive K-correction for distant objects implied by the steeply rising spectra. Indeed, very high- z sources, most of which associated to active objects, have been recently detected at the millimeter (both in the continuum and line emission; see e.g. Andreani et al. 1993; Isaak et al. 1994; Chini & Krügel 1994; Dunlop et al. 1994; Barvainis et al., 1994; Yamada et al., 1995). This allows estimates of the barionic content in the ISM at such high redshifts.

A further reason for our interest in this waveband domain is that an astrophysical background of extragalactic origin may be observable here, given the minimal influence of the foreground emissions (due to interplanetary dust and dust in the Galaxy). The detection of an extragalactic sub-

mm background would allow to directly probe such early epochs, if single sources were too faint for detection because of the high redshift or low intrinsic luminosity.

The existence of a cosmological background distinct from the Cosmic Background Radiation (CBR) has been widely discussed in the past (Partridge & Peebles 1967; Tinsley 1973; Stecker, Puget & Fazio 1977; Rowan-Robinson, Negroponte & Silk 1979; Negroponte 1986; Bond, Carr & Hogan 1986, 1991). It has been expected to arise either from the integrated emission of unresolved proto-structures – such as primeval galaxies, population III stars, or other sources of pregalactic origin and thermal emission produced by associated coeval dust. Many observational efforts have been devoted to detect it, (e.g. Matsumoto et al. 1988), and sometimes controversial results were reported, mainly because of the uncertain subtraction of the local foregrounds implied by the very limited sky coverage.

For background signals with spectra different from that of the Galaxy, strong limits on the associated energy density in the wavelength range $500 < \lambda < 5000\mu m$ have been set by the COBE-FIRAS data. The observational constraints on deviations from a pure blackbody spectrum of the CBR (0.03% in brightness) imply limits to the integrated energy density of $\Omega_{R,FIR} h^2 \leq 10^{-7}$ (i.e. $\nu I_\nu <$

$4.1 \cdot 10^{-9} \text{ W m}^{-2} \text{ sr}^{-1}$; Wright et al. 1994; Fixen et al., 1996; Burigana et al. 1996).

The interest in long-wavelength background searches was recently renewed by the claim by Puget et al. (1996) of a tentative detection in the all-sky COBE-FIRAS data of an isotropic signal which can be ascribed to an extragalactic source. An isotropic cold component, with a spectrum similar to that of the Galaxy – and not inconsistent with the Puget’s et al. background – appears to have been detected by the COBE team itself (Fixen et al., 1996). The intensity of this background comes impressively close to the level predicted for evolving extragalactic sources (Franceschini et al. 1994).

It will be of great significance not only to confirm or disprove this result with further space observations (e.g. by the ISO and IRTS missions), but also to eventually characterize the source populations originating it via dedicated deep surveys in the sub-millimeter atmospheric channels accessible from ground.

Last, but not least, mappings of the Cosmic Background Radiation down to a few arcminute scale, that will be performed over a wide wavelength interval around the millimeter to investigate the cosmic structure at the decoupling, will have to account for spurious signals due to the integrated emissions of *mm* and sub-*mm* sources. The case for a variety of dedicated balloon and planned space missions (e.g. the ESA’s COBRAS-SAMBA and NASA’s MAP) heavily relies on the estimated levels of foreground anisotropies.

Most of the estimates published so far are based on the assumption that the long-wavelength spectrum of the Galaxy, as detailed by the COBE mission, is a representative one for normal galaxies (Blain and Longair, 1996; Gawiser and Smoot, 1996). As discussed by Franceschini & Andreani (1995), the Galaxy spectrum seems to include relatively large amounts of cold dust, as typical of inactive disk galaxies with low star-formation activity. Then it may not accurately describe the other component of the IRAS galaxy population, i.e. actively star-forming objects with warmer spectra on average and steeper sub-mm slopes.

As a contribution to the understanding of the extragalactic sky at millimetric wavelengths, and in the perspective of optimizing and interpreting future mm and sub-mm observations, this paper reports on a detailed statistical discussion of the *mm* emissivity properties of galaxies. This analysis is based on observations of the 1.25 *mm* continuum emission from a complete sample of IRAS galaxies obtained with the SEST Telescope.

The combination of IRAS and *mm* photometric data already allowed us to study galaxy spectra in this energy domain and to quantify the presence of dust in galaxy discs (Franceschini & Andreani 1995; Andreani & Franceschini 1996). Now the use of a complete flux-limited sample allows us straightforward determinations of IR-mm bivariate luminosity distributions, of *mm* luminosity functions and volume emissivities. Our choice of a far-IR selected reference sample, rather than of an optical one, allows us an unbiased sampling of the whole phenomenology of dust effects in galaxies.

In Section 2 we summarize information on the dataset, mention our *mm* observations and discuss some flux correlations. In Section 3 we derive the FIR-*mm* bivariate luminosity distribution, and the 60 and 1250 μm luminosity functions. The far-IR/mm volume emissivity of galaxies, their

contribution to the cosmic infrared background (CIRB), and implications for future sub-mm surveys are discussed in §4.

A Hubble parameter of $H_0 = 50 \text{ Km/s/Mpc}$ is used throughout the paper.

2 THE DATASET

2.1 The far-IR selected sample and *mm* observations

The galaxy sample used in this work was selected from the IRAS Point Source Catalogue and is complete and flux limited to $S_{60\mu\text{m}} = 2 \text{ Jy}$ within an area of 0.133 steradians. Complete information exists also for distances (mostly from distance indicators), optical magnitudes and sizes. It includes 30 galaxies with morphological types from S0/a to Scd, and distances ranging mostly from 18 to 250 Mpc. Exceptional objects are NGC 253 (at a distance of 3.6 Mpc) and a type-2 Seyfert galaxy found at 471 Mpc. Further details on the sample objects can be found in Andreani & Franceschini (1996), AF96 hereafter.

The selection area avoids peculiar galaxy concentrations or voids, and provides a representative section of the local universe. This, and the sample completeness, are checked through the volume test: the global average is $\langle V/V_{\text{max}} \rangle = 0.45 \pm 0.06$. Average volume ratios within 60 μm luminosity bins are reported in Table 1: no significant departures from the expected value of 0.5 are found.

The sample has been observed at 1.25 *mm*, during various campaigns, with the ESO-SEST telescope at La Silla, equipped with a sensitive ^3He -bolometer. The SEST was chosen as providing a good compromise between detector sensitivity and spatial coverage, allowing to minimize the corrections for beam-aperture. Twenty-one objects have been detected at better than 3σ , while for the nine undetected significant upper limits to the *mm* flux are set.

As discussed in previous reports, the basic uncertainty in our *mm* photometry is due to the corrections for beam-aperture implied by the finite size of the sources compared to the diffraction-limited beam size. This implies a differential effect, in the sense that the nearest larger galaxies, which are also the less luminous on average, are subject to the largest flux correction. Then, in the comparison with the total fluxes provided by IRAS, the whole FIR-mm relationship (slope and normalization) may be affected.

Lacking imaging information on the millimeter surface brightness distributions, Franceschini & Andreani (1995, hereafter FA95) and AF96 have tried to infer statistical aperture corrections from analyses of the average mm to FIR flux ratios versus distance and galaxy size. This, however, has not solved the problem of defining reliable aperture corrections: two different solutions are still viable, one implying a somewhat more compact distribution of cold dust in spiral galaxies with respect to that of optical starlight emission, that we have interpreted as due to a radial gradient of metallicity in galactic disks. The other assuming a roughly equal distribution of dust and stars, which implies a mm to FIR flux ratio decreasing with galaxy luminosity.

The corresponding beam-aperture correction for our SEST flux data would be small (30% on average) in the former case, while being typically a factor 2 in the latter.

Figure 1. Correlations of the 1250 μm to the 100 μm and 0.44 μm (B-band) fluxes. The millimeter fluxes are aperture-corrected according to hypothesis (a) (see text).

Very limited progress in the field of *mm* photometry, based on direct imaging at long wavelengths and indirect inferences of dust extent in galaxies from optical/near-IR data, has been achieved in the meantime. No conclusive results are either expected, until large multi-channel bolometer assemblies will be used in mapping representative samples of galaxies, which requires full operation by e.g. the SCUBA bolometer array on JCMT and by the MPI arrays on IRAM and SEST. Our subsequent analysis of *mm* properties of galaxies will account for such uncertain aperture correction by considering both above mentioned possibilities: that the millimetric scale-length is one third of the optical ($\alpha_{mm} = \alpha_o/3$) or just equal to ($\alpha_{mm} = \alpha_o$). This should confidently bracket the likely real situations. For conciseness, we will refer in the following to the former as hypothesis (a), and to the latter as hypothesis (b).

Detailed descriptions of the observations and data processing, together with the the IRAS and *mm* photometry, are reported by FA95, Andreani, Casoli & Gerin (1995), and AF96. We conclude by stressing that the sample has nice properties of completeness and is then suited for various kinds of statistical tests.

2.2 Flux and luminosity correlations

The far-IR and *mm* emission in normal galaxies are due to re-processing by dust in the ISM of the starlight background. We then expect the corresponding flux densities to be correlated. Since the 60 and 100 μm channels are interpreted as coming from two partly distinct components, i.e. warm dust in star forming regions and cold widespread dust illuminated by the general galactic background, we expect that the long wavelength *mm* emission to be better correlated with the 100 μm one. On the contrary, the correlation with the optical emission is expected to be poor.

All this is fairly well supported by our data. Correlation plots of *mm* fluxes and luminosities with FIR and optical emissions are shown in Figures 1 and 2. We find the *mm* emission for our sample galaxies to be correlated with the 60 and 100 μm ones. The corresponding flux correlations are significant at 3.5σ and 4.6σ if we adopt hypothesis (a)

above (i.e. stronger concentration of dust). Under hypothesis (b) (equally distributed dust and light), the flux correlations are more significant (4.2σ and 6σ , respectively), because brighter and larger galaxies have a greater correction for aperture (Fig.1a). We see in Fig. 1b that the regression of the *mm* to optical flux is significantly flatter, with the 1.3 *mm* flux barely dependent on the optical magnitude, as expected.

For obvious reasons, luminosity plots show stronger correlation. As an example, we report in Figure 2 plots of the 100 μm ($L_{100\mu m}$) versus 1.3 *mm* ($L_{1250\mu m}$) luminosity for three different assumptions about the dust extent (hypotheses [a] and [b], and no aperture correction). High correlation significances ($\sim 10\sigma$) are found in all cases. As noted above, the slope of the *mm*-FIR correlation depends on the adopted aperture correction. A precisely linear scaling is found from hypothesis (a), with a best-fit regression:

$$L_{1250\mu m} (erg/s/Hz) = 6.0 \cdot 10^{-3} L_{60\mu m} (erg/s/Hz), \quad (1)$$

or

$$\nu_{1250} L_{1250\mu m} (L_{\odot}) = 2.9 \cdot 10^{-4} \nu_{60} L_{60\mu m} (L_{\odot}).$$

According to the hypothesis (b), the regression becomes non-linear, favouring higher far-IR emission over the *mm* one at the higher luminosities:

$$\log(\nu_{1250} L_{1250\mu m} [L_{\odot}]) = -1.75 + 0.85 \log(\nu_{60} L_{60\mu m} [L_{\odot}]). \quad (2)$$

Such non-linear behaviour may be interpreted as due to the brighter radiation field rising the dust temperature and shifting the peak emission to shorter wavelengths.

These correlation studies account also for the fraction of sources with only an upper limit on the *mm* flux. A *survival analysis* technique has been used to test logarithmic plots in the presence of upper limits. The best-fitting and the correlation coefficients, with their uncertainties, are computed using a method developed by Schmitt (1985), accounting for arbitrarily censored data. A bootstrap technique (with typically 1000 replications) is used to estimate the uncertainties. Details on the application of the method can be found in Franceschini et al. (1988).

A tight correlation of the millimetric emission with the far-infrared one, which is expected on the basis of the physical interpretation for the emission source, is then confirmed by our observations. This justifies the effort, that will be pursued in the next Section, to study the millimetric emission properties of galaxies starting from a far-infrared selected sample.

3 THE MILLIMETER LUMINOSITY FUNCTION

A precise knowledge of the local luminosity function (LF) of galaxies is essential to derive all basic statistics of a source population. In particular, matched to number count estimates and to measurements of the diffuse background at the same wavelength, it is needed to understand the evolution properties of the population.

To estimate the millimetric LF of galaxies we have made use of the 60 μm -selected sample described Sect 2. This selection wavelength was chosen to minimize the contamination from galactic cirrus (relevant at 100 μm), and from stars

Figure 2. Correlations of the 1.25 mm to 100 μm luminosities (νL_ν in solar luminosities), for three different assumptions about the extent of the millimetric emission. Best-fit values for the regression slopes for the three cases of no-correction, $\alpha_{mm} = \alpha_o/3$ and $\alpha_{mm} = \alpha_o$ are in the order: slope=1.25 \pm 0.25; slope=0.99 \pm 0.15; slope=0.85 \pm 0.19.

at shorter wavelengths. For the same reasons, most of the previous analyses of LF's for IRAS galaxies have referred to the 60 μm selection (e.g. Lawrence et al. 1986; Saunders et al. 1990).

3.1 The bivariate FIR-mm luminosity distribution

As a step towards a mm LF, we need to estimate the conditional probability distribution to observe luminosities $L_{1250\mu\text{m}}$ in a given interval from galaxies with any given far-IR luminosity $L_{60\mu\text{m}}$. We have divided the plane $\log L_{1250\mu\text{m}} - \log L_{60\mu\text{m}}$ into a 6x6 matrix, each element of which corresponding to a half-magnitude interval in both luminosity scales. We have then estimated the bivariate probability distribution into the 6x6 matrix bins in the following way. For each $L_{60\mu\text{m}}$ bin, we have computed the probability distribution to observe a value of $\log L_{1250\mu\text{m}}$, differentiated into 6 bins of $\log L_{1250\mu\text{m}}$. Such differential distributions have been computed through the Kaplan-Meier estimator (e.g. Schmitt, 1985), to account for the upper limits on $L_{1250\mu\text{m}}$.

The results of this calculation appear in Table 1, together with information on the number of sources per bin, the V/V_{max} test, and the FIR and mm LF. The mm data in Table 1 have been corrected for aperture according to model (a) in Sect. 2.1. A strong correlation of the two luminosities is clearly apparent, as in the plots of Fig. 2. As a check of the border effects implied by a 2D binning of a small sample, we have repeated the operation with a 5x5 matrix, and found no systematic deviation in the final mm LF.

3.2 Luminosity functions of galaxies at

$\lambda = 1250 \mu\text{m}$ and $\lambda = 60 \mu\text{m}$

We have derived the 60 μm LF for our galaxy sample using the generalized Schmidt's estimator $1/V_{max}$, and adding the contributions of sources to the volume density in each $\log L_{60\mu\text{m}}$ -bin. The results are also reported in Table 1.

Knowing the conditional probability distribution of $L_{1250\mu\text{m}}$ at given $L_{60\mu\text{m}}$ and the 60 μm LF, the millimetric LF is simply found by adding together volume densities contributed by objects in all $\log L_{60\mu\text{m}}$ -bins, at constant $\log L_{1250\mu\text{m}}$ (see again, for further details on this procedure, Franceschini et al. 1988).

Figure 3a compares our derived 60 μm LF (open squares) with that previously determined by Saunders et al. (1990) (filled squares). We see quite a good match between the two, which confirms the statistical quality of our, yet small, far-infrared sample.

Figure 3b summarizes our results on the millimetric LF of galaxies. Outcomes of various statistical procedures are compared here to infer a safer and most unbiased LF, and to have an idea of the uncertainties in it.

Open squares in Fig. 3b mark the two values of the LF obtained from our 60 μm LF combined with our bivariate luminosity distribution: the lower value comes from the assumption of type-(a) aperture correction ($\alpha_{mm} = \alpha_o/3$), the upper one from type-(b) correction ($\alpha_{mm} = \alpha_o$). We see that the difference is quite important only in the bin at $\log L_{1250\mu\text{m}} = 41.6$, partly due to a bad effect of the binning.

Filled squares in Fig. 3b are estimated as the open squares, but starting from the 60 μm LF of Saunders et al. (1990) instead of the one inferred from our galaxy sample. The two estimates are quite in agreement, except for the highest luminosity datapoint, due to our lack of far-IR sources there. Because of the small number of sources and poor statistics of our sample, we judge this filled-square estimate to be a more precise evaluation of the millimetric LF of galaxies.

The continuous line in Fig. 3b is the predicted LF, obtained from a best-fit to the Saunders's et al. 60 μm LF (continuous line in Fig. 3a) and transformed to 1250 μm with the average luminosity ratio of eq. (1), i.e. the best-fit value under hypothesis (a). The dotted line is obtained from the Saunder's et al. LF transformed according to the non-linear regression of eq. (2).

We see that, in spite of the limited statistics of our sample and some systematic uncertainties, the overall shape of the millimetric LF is relatively well defined. We report in Table 2 our best-guess LF with its global confidence interval.

As a final warning, our procedure to estimate a LF from the bivariate luminosity distribution yields, in principle, only a lower limit to it, because of the possible unaccounted contributions of faint far-IR sources with relatively strong mm flux. This might be a problem, in particular, at the faint end of the LF, but could only be tested through direct inspection of selected areas with mm imagers. This will not be an easy job even with large-format bolometer arrays, as we discuss below.

4 GALAXY CONTRIBUTIONS TO THE FAR-IR AND MM SKY

The knowledge of the LF allows a precise estimate of the long-wavelength volume emissivity of galaxies. We discuss in this § three related applications, concerning the contribution to the extragalactic far-IR/mm background intensity, the small-scale sky signals induced by a random space distribution of galaxies, and predictions for source selections

Figure 3. The local luminosity functions at $60 \mu m$, compared with published data (panel [a]), and at $1250 \mu m$ (panel [b]), estimated from our IRAS galaxy sample. Open boxes in panel (b) are based on our new $60 \mu m$ LLF, whereas the filled ones are based of the Saunders’s et al. LLF. The continuous line is the $1250 \mu m$ function transformed from the $60 \mu m$ one through a constant L_{1250}/L_{60} ratio as in eq. (1). The dotted line is the same, but from the non-linear scaling of eq. (2).

in the sub-millimeter. This may prove useful for currently planned and future experiments in this field.

4.1 Contributions to the CIRB’s intensity

The mm and far-IR LF, together with the average far-IR to mm broad-band spectrum of galaxies as discussed in FA95 and AF96, allow a largely model-independent estimate of the minimal contribution of galaxies to the IR-mm extragalactic background (BKG). This corresponds to a sort of *known baseline* for the CIRB, any positive evolution effects (i.e. any increase of the population emissivity with redshift) adding some amount of flux to such a baseline.

On quite general grounds we may write the contribution of the galaxy population to the background intensity at a given IR wavelength as:

$$I_{CIRB}(\nu) = \frac{1}{4\pi} \frac{c}{H_0} \int_0^{z_{max}} dz (1+z)^{-5} (1 + \Omega_0 z)^{-0.5} j_\nu(z) \quad (3)$$

where $\Omega_0 = 2q_0$ and where the redshift-dependent comoving volume emissivity is given by

$$j_\nu(z) = \int_{L_{min}}^{L_{max}} d \log L_{FIR} L_{FIR} \rho_0(L_{FIR}) \cdot E(L_{FIR}, z) K(L_{FIR}, z) \quad (4)$$

which involves the local LF, $\rho_0(L_{FIR})$, the evolutionary correction $E(L_{FIR}, z)$ and the K-correction $K(L_{FIR}, z) = L[\nu(1+z)]/L(\nu)$. For well-behaved LF’s, i.e. LF’s quickly converging at high L and flat at low L as in our case, the integral in eq.(4) depends quite moderately on L_{min} and L_{max} .

For a population of non-evolving objects [$E(L_{FIR}, z) = 1$], the CIRB is mostly contributed by local ($z < 1$) objects

Figure 4. Contributions of galaxies to the extragalactic BKG. The lower shaded region marks our estimated minimal background (see text), compared to the, arbitrarily normalized, average spectrum of local galaxies (AF96, thick continuous line). The upper thick line is the background flux level from our luminosity evolution model. The upper shaded region is the estimated extragalactic background by Puget et al. (1996). Data points are from Hauser (1994) and Fixen et al. (1996).

and the volume emissivity simplifies to the local value

$$j_\nu(z) \rightarrow (1+z)^{\alpha_{mm}} j_\nu(0),$$

$$j_\nu(0) = \int d \log L_{FIR} L_{FIR} \rho_0(L_{FIR}).$$

where the z-dependent factor is the K-correction for moderate redshift sources, which is non negligible for such steeply rising mm spectra ($\alpha_{mm} \simeq 3.5$, AF96).

Since the population emissivity is expected to be larger in the past when the rate of star-formation is usually observed to be stronger, a lower limit to the contribution of the population to the CIRB is found by putting in eq. (3) $z_{max} = 1$, $E(L, z) = 1$, and $j_\nu(z) = (1+z)^{\alpha_{mm}} j_\nu(0)$. Note that this limit only depends on a reliable definition of the LF, that we have conservatively taken from the continuous line of Fig. 3b (case [b], small aperture corrections).

The minimal galaxy BKG is shown in Figure 4 as the lower shaded region: given the above assumptions, the real extragalactic BKG is quite likely in excess of this. Note that, because of the strong K-correction effect for even such low-z objects, this spectrum is broader than the average long- λ spectrum of local galaxies as defined by AF96 (and proportional to the volume emissivity $j_\nu[0]$).

The data points in Fig. 4 have been measured by the DIRBE and FIRAS experiments on COBE (Hauser 1994; Fixen et al. 1996). The upper shaded region is a recent estimate of the extragalactic BKG in the sub-mm cosmological window. From a careful subtraction of the galactic "cirrus" emission exploiting a new HI survey, Puget et al. (1996) have been able to recover this isotropic flux, which was shown to be not of Galactic nor of solar origin. A residual isotropic flux, consistent with the Puget’s et al. determination, has been recently determined by Fixsen et al. (1996) after subtraction from the observed FIRAS maps of the CBR Planck blackbody spectrum, the dipole and the Galactic contribu-

tion. The authors attribute this residual to a Galactic cold ($T = 9$ K) halo or to an extragalactic component. Altogether, in spite of the uncertain interpretation, an isotropic cold residual component of likely extragalactic origin has been detected by independent groups.

An important effect can be noticed by comparing the observed background to our expected level from non-evolving galaxies: there is a wide margin between the observed flux and our minimal BKG. This result is quite robust. The predicted no-evolution spectrum would only marginally increase (by less than a factor 2) if we would adopt the dotted line LF in Fig. 3b, corresponding to the larger case (b) flux corrections.

This result may be interpreted in terms of either a strong evolution with cosmic time of the same locally observed source populations, or of a bright new one emerging at high redshifts. In either case, *an enhanced past activity of galaxies at such wavelengths seems required to fill in the observed gap between the contribution of local galaxies and the COBE residual background.*

The predicted spectrum by a model of galaxy luminosity evolution is shown in Figure 4. The model involves two independent contributions, from an early dust-enshrouded phase during the formation of early-type galaxies (as discussed by Franceschini et al. 1994) and from enhanced star-formation activity at moderate redshifts in later-type systems (see Danese et al. 1987; Rowan-Robinson et al. 1993) due to interactions. This model provides an accurate description of the sub-mm extragalactic background.

In principle, a comparison between the local emissivity $j_\nu(0)$ and the CIRB spectrum allows inferences about the average redshift of the emitting sources and their evolutionary pattern. In practice, uncertainties may be introduced by the evolution with cosmic time of the dust temperature distribution. A detailed comparison of the observed background and model expectations will be discussed separately (Burigana et al., 1996).

4.2 Small-scale anisotropies of the infrared background and predictions for source selection

A way to test the origin of the inferred extragalactic background at sub-mm wavelengths is to look for the anisotropy structure in its surface brightness distribution. If the bulk of the emission comes from relatively bright sources (e.g. high-redshift galaxies in a transient luminous phase) some signals are expected at small angular scales. We discuss in this Section prospects for ground-based observations by current instrumentation.

Anisotropy signals induced by a random sky distribution of sources of known LF are easily computed from published formalism (Condon, 1984; Franceschini et al. 1989; see De Zotti et al. 1996 for a complete treatment). We quantify the contribution of galaxies to the CIRB's small-scale anisotropies through the probability distribution function $P(D)$ of the integrated sky signals D (e.g. in Jy/pixel) obtained from a sampling of the sky with an angular resolution element (pixel) of area A (e.g. in square arcsec).

The basic procedure to compute $P(D)$ is to perform a first integral of the LF on redshift to get the differential source counts, followed by a second integration over the

Figure 5. Probability distributions of integrated sky signals for representative survey experiments. The dashed lines are the expected $P(D)$ for extragalactic sources. Heavy lines reproduce gaussian instrumental (and atmospheric) noise. Dotted lines are the convolution of the instrumental and confusion noise distributions, while the histogram with (Poisson) errorbars correspond to a sampling of 1000 independent sky pixels. The 4σ source detection limit, derived with an iterative procedure, is marked with an arrow. Panel (a) simulates an experiment performed at $\lambda = 1300$ μm with IRAM, 19 channel array, of 50 integrations of 10 h (rms noise of 0.3 Jy). Luminosity evolution model. Panel (b) is for SCUBA at JCMT, 27 integrations of 4 h (rms noise of 0.3 Jy). Luminosity evolution model. Panel (c) is the same as panel (b), for the case of no galaxy evolution.

beam area A to get the cumulative signals of all sources in a beam, for a given beam profile. Observations at such long wavelengths will be in most cases diffraction-limited, and a gaussian function is assumed to fit the inner Airy distribution. The gaussian width is parametrized by its full-width at half-maximum θ .

We report in Figure 5 a few simulated $P(D)$ distributions of sky signals for representative survey experiments. Adopted here for an illustration purpose is the luminosity evolution model discussed in the previous §, which has indicated by Puget et al. (1996) as one best fitting the COBE isotropic sub-mm flux.

Obvious reference wavelengths for observations from ground are $\lambda = 1300$, 800 and 450 μm (see Franceschini et al. 1991 and Blain and Longair 1996, for discussions on the relative merits of various combinations of sky area vs. wavelength and sensitivity). The adopted resolution elements at $\lambda = 450$ and 800 μm correspond to the limit of diffraction for a 15m telescope (e.g. JCMT), while for $\lambda = 1300$ they correspond to a 30m dish (e.g. IRAM). In any case, the approximate scaling of the total deflection D in the pixel (x-axis of Figure 5), for different pixel areas A and survey wavelengths λ , is simply given by:

$$D(A, \lambda) = D_0(A_0, \lambda_0) (A/A_0) \cdot (\lambda/\lambda_0)^{-3.5},$$

with obvious meaning of the symbols. The scaling with wavelength comes from our (AF96) fit to the average far-IR/mm galaxy spectrum.

The expected sky signals from extragalactic sources, as described by the $P(D)$ (dashed lines), are compared in Fig. 5 with gaussian distributions reproducing the instrumental

noise, for the various experiments (heavy line). The gaussian widths correspond to long integrations, of typically several hours per pixel. The convolution of the instrumental and confusion noise distributions (dotted line) simulates the total expected signals for realistic surveys and allows a precise evaluation of the source detection limit S_{lim} . For the latter we have assumed the flux corresponding to 4 times the standard deviation σ of the convolved distribution. The procedure to compute it is an iterative one (see Franceschini et al. 1988): an high value for S_{lim} is first assumed, and σ determined by putting $P(D) = 0$ for $D > S_{lim}$; S_{lim} is then lowered, until it equals the 4σ value. Down-pointing arrows mark in Fig.5 detection limits estimated with this procedure.

Figure 5 emphasizes the difficulty of dedicated deep extragalactic surveys in the sub-millimeter, even with the currently most sensitive equipments. The typical extragalactic signals expected from evolving sources are largely dominated by the instrumental noise at $1300 \mu m$ and by the atmospheric noise at $450 \mu m$, even for very long integrations.

The errorbars overimposed on the histograms of the convolved distribution correspond to the Poisson expectation for a total of 1000 independent sky pixels. This figure is kept constant for all simulated experiments. Fig. 5a simulates a $1300 \mu m$ survey with a 19 channel bolometer system on IRAM, using 50 integrations of 10 hours each (perhaps corresponding to a rms noise of 0.3 mJy), for a total integration time as large as 500 h. Above the 4σ detection limit ($S_{lim} = 1.3$ mJy), of order of only 3 evolving galaxies would be expected, while the simulated deflection distribution does not deviates significantly from the gaussian noise distribution.

Fig. 5b refers to a $850 \mu m$ survey with the 37 channel SCUBA array on JCMT, performing 27 integrations of 4 hours each (rms noise of 0.3 mJy for very good weather conditions; total integration time of 110 hours). Above $S_{lim} = 2.2$ mJy, some 15 galaxies could be detected, if cosmic evolution is as strong as assumed here.

Not reported in Fig. 5, a $450 \mu m$ survey with the 91 channel SCUBA array would be, for any reasonable integration time, limited by atmospheric noise (the expected extragalactic 1σ width of $P(D)$ is 0.4 mJy, compared to several mJy of instrumental noise reached with many hours of integration). For a total integration time of 100 hours and 4 hour exposure per pixel, some 4 galaxies would be found, and no significant signal in the deflection distribution above the (largely atmospheric) noise.

Only at $850 \mu m$ (Fig. 5b) the extragalactic signal and detector noise may be comparable, as shown by the long tail at large D values. Detailed best-fitting to the observational distribution will allow to extend the estimate of the sub-mm source counts significantly below the detection limit and down to $S_{850} \simeq 0.5$ mJy. Even in such case, however, no evolution for galaxies would imply that the SCUBA survey would again be detector noise limited (see Fig. 5c) and that as few as 3 galaxies be detected at $S > S_{lim} = 1.2$ mJy in 100 hours of observation.

5 CONCLUSIONS

Exploitation of a bright complete sample of IRAS galaxies has allowed us to derive a relatively well defined millimetric

luminosity function of galaxies, in spite of a residual uncertainty on the beam-aperture corrections, which has been modeled.

The knowledge of the volume emissivity of local galaxies allowed us to compute a model-independent estimate of the galaxy background under the assumption of no evolution. This minimal background was found to keep much below the recently measured intensity of the extragalactic flux by Puget et al. (1996) (perhaps confirmed by Fixsen et al., 1996).

We then inferred that a marked evolution with cosmic time of galaxy long-wavelength emissivity is required to explain the observed background level. Alternative possibilities would be an entirely new source population turning on at faint fluxes, or a diffuse emission process, perhaps operating at high redshifts.

We have addressed the question of how (and if) these proposed solutions may be tested by sub-mm observations from ground, before the advent of dedicated space-born instrumentation. Interesting perspectives are provided by deep surveys of small selected areas with multi-channel arrays, to derive samples of mm sources and to analyse the small-scale anisotropy signals.

Our analysis, based on the observed millimetric properties of IR selected galaxies, has shown the difficulty of sub-mm extragalactic observations from ground. The most promising chance is soon provided by the very sensitive JCMT-SCUBA bolometer array at $850 \mu m$, which could detect (or put upper limits on) evolving galaxies. At other wavelengths, and for less competitive observational setups, the chances to perform successful surveys are much lower. Perhaps only dedicated space missions (e.g. FIRST), or the exploitation of millimetric terrestrial sites even more extreme than those currently in use (e.g. the Antarctic Domes) could eventually allow them.

Acknowledgements We are grateful to G. De Zotti and J.L. Puget for helpful discussions. This work has been partly funded by ASI Contract 95-RS-116.

REFERENCES

- Andreani P., La Franca F, Cristiani S., 1994, MNRAS 261, L35
- Andreani P., Casoli F. and Gerin M., 1995, A&A 300, 43
- Andreani P. & Franceschini A. 1996, MNRAS in press.
- Barvainis R., Tacconi L., Antonucci R., Alloin D., Coleman P., 1994 Nat 371, 586
- Blain A.W. & Longair M.S. 1993, MNRAS 264, 509
- Bond J.R., Carr B.J. & Hogan C.J., 1986, ApJ 306, 428
- Bond J.R., Carr B.J. & Hogan C.J., 1991, ApJ 367, 420
- Burigana, C., Franceschini, A., Mazzei, P., Danese, L., De Zotti, G., 1996, in preparation
- Chini R., and Krügel E., 1994, A&A 288, L33
- Condon J.J., 1974, ApJ 188, 279
- Dunlop J.S., Hughes D.H., 1994 Nat 370, 347
- Danese L., De Zotti G., Franceschini A., Toffolatti L., 1987, ApJ 318, L15
- De Zotti, G., Franceschini, A., Toffolatti, L., Mazzei, P., Danese, L.: 1996, *Astro. Lett. and Communications*, in press.
- Fixsen et al., 1996, COBE-preprint 96-11
- Franceschini A. & Andreani P. 1995, ApJ 440, L5
- Franceschini A., Danese L., De Zotti G., Toffolatti L., 1988, MNRAS 233, 157

- Franceschini A., Toffolatti L., Danese L., De Zotti G., 1989, ApJ 334, 35
- Franceschini A., Toffolatti L., Mazzei P., Danese L., De Zotti G., 1991 A&AS 89, 285-310
- Franceschini A., Mazzei P., De Zotti G., Danese L., 1994, ApJ 427, 140
- Franceschini A., Granato G., Mazzei P., Danese L., De Zotti G., 1995, in *Unveiling the Cosmic Infrared Background*, College Park, Maryland, AIP Conference Proceedings, E. Dwek Ed., 159.
- Gawiser E. & Smoot G.F., 1996 preprint
- Hauser M. 1994 in *Examining the Big Bang and Diffuse Background Radiations*, IAU symp. 168, The Hague, The Netherlands
- Isaak K.G., McMahon R.G., Ellis R.E., Withington S., 1994, MNRAS 269, L28
- Lawrence A., Walker D., Rowan-Robinson M., Leech K.J., Penston M.V., 1986, MNRAS 219, 687
- Matsumoto T., Hayakawa S., Matsuo H., Murakami H., Sato S. Lange A.E., Richards P.L. 1988, ApJ 329, 567
- Negroponte J., 1986, MNRAS 222, 19
- Partridge R.B. & Peebles P.J., 1967, ApJ 148, 377
- Puget J.L., et al., 1996, A&A 308, L5
- Rowan-Robinson M., Benn, C., Lawrence, A., McMahon, R., Broadhurst, T., 1993, MNRAS 263, 123
- Saunders W., Rowan-Robinson M., Lawrence A., Efstathiou G., Kaiser N., Ellis R.S. & Frenk C.S., 1990, MNRAS 242, 318
- Schmitt J., 1985, ApJ 293, 178
- Stecker F.W., Puget J.L. & Fazio G.G., 1977, ApJ 214, L51
- Tinsley B., 1973, A&A 24, 89
- Yamada T., Aoki K., Tomita A., Takata T., Ohta K., Yoshida M., 1995, ApJ 438, L5
- Wright E. L. et al. 1994, ApJ 420, 450

Table 1. FIR and mm local luminosity function, and the

bivariate luminosity distribution

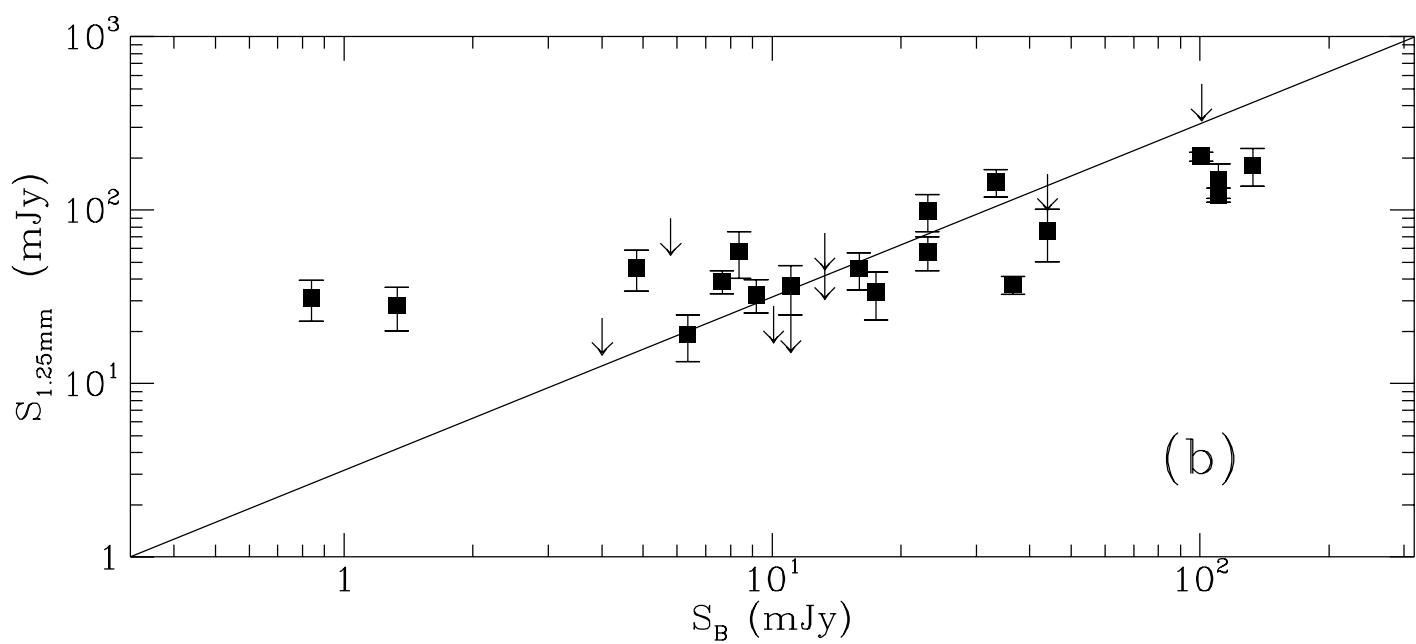
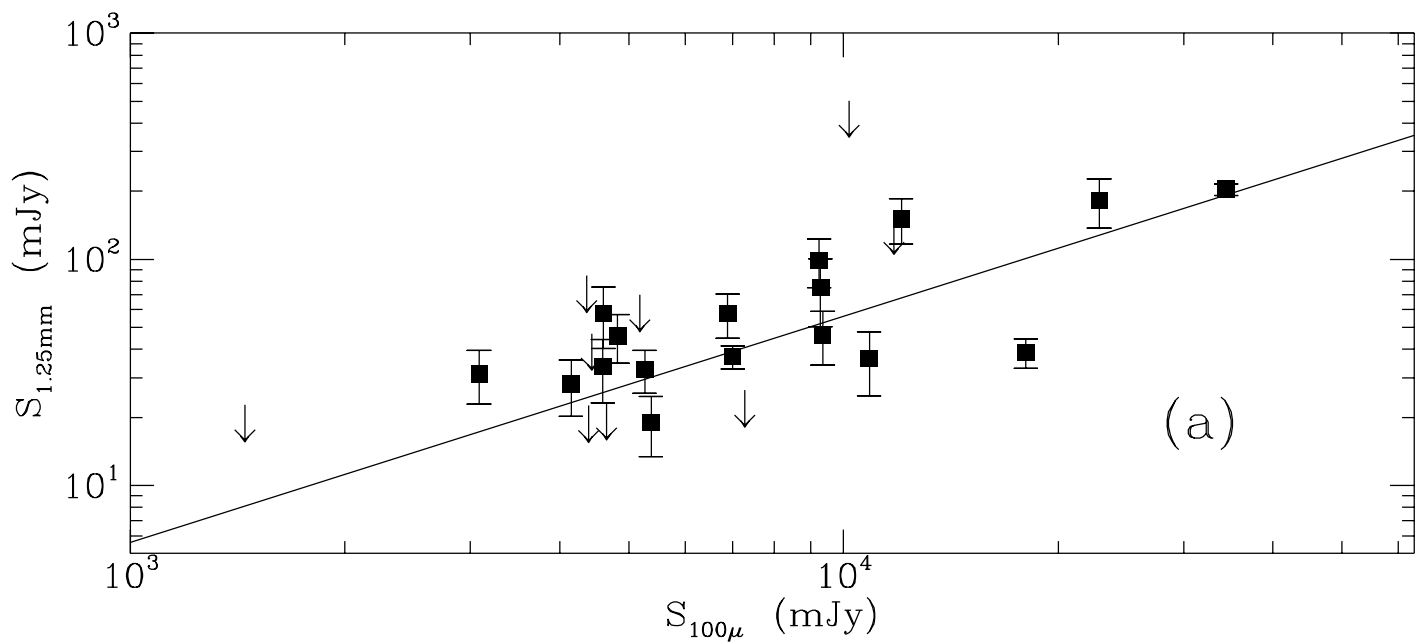
$\log L_{60\mu}$ (erg/s/Hz)	30.75	31.25	31.75	32.25	32.75	33.25
$\rho_o(Mpc^{-3}\Delta \log L_{60\mu})$	$1.77 \cdot 10^{-3}$	$2.43 \cdot 10^{-4}$	$1.13 \cdot 10^{-4}$	$1.83 \cdot 10^{-5}$	$2.52 \cdot 10^{-6}$	$3.15 \cdot 10^{-8}$
1σ error	$9.64 \cdot 10^{-5}$	$2.51 \cdot 10^{-5}$	$2.82 \cdot 10^{-6}$	$7.87 \cdot 10^{-7}$	$2.20 \cdot 10^{-7}$	$3.15 \cdot 10^{-8}$
$\langle V/V_{max} \rangle$	0.549	0.521	0.485	0.403	0.605	0.830
# of sources per bin	6	4	9	6	4	1

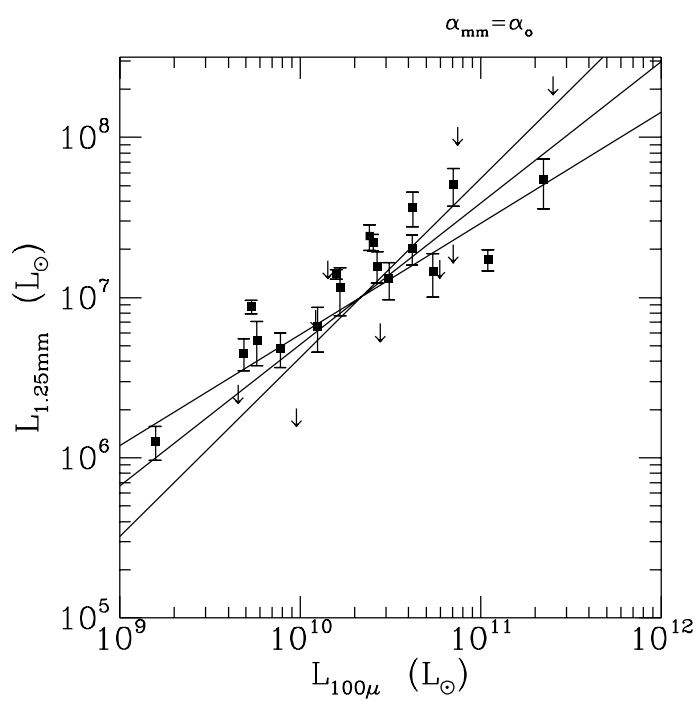
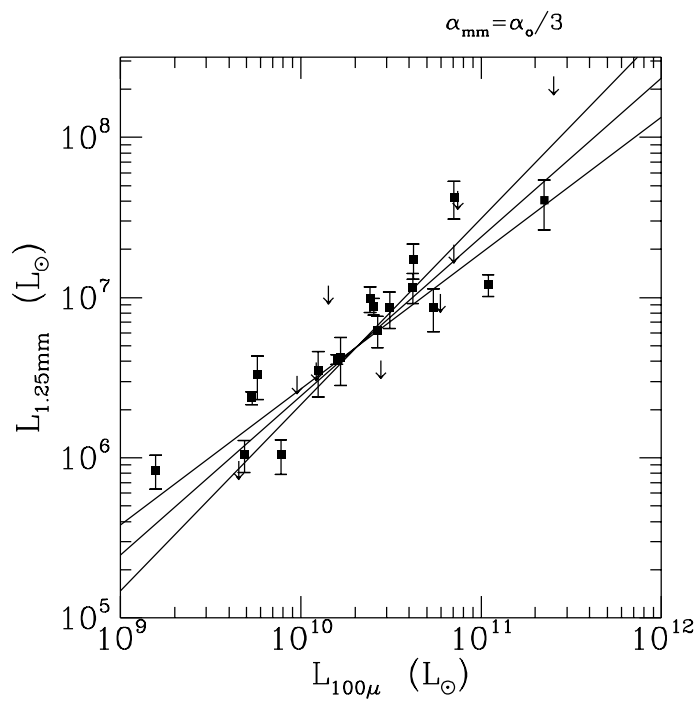
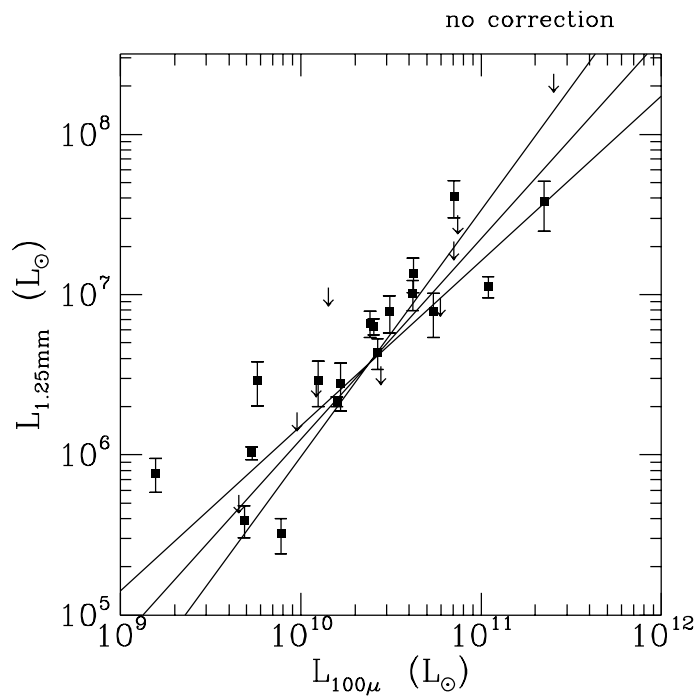
Bivariate luminosity function of the 1.3mm to 60 μm luminosities
($Mpc^{-3}\Delta \log L_{60\mu}$)

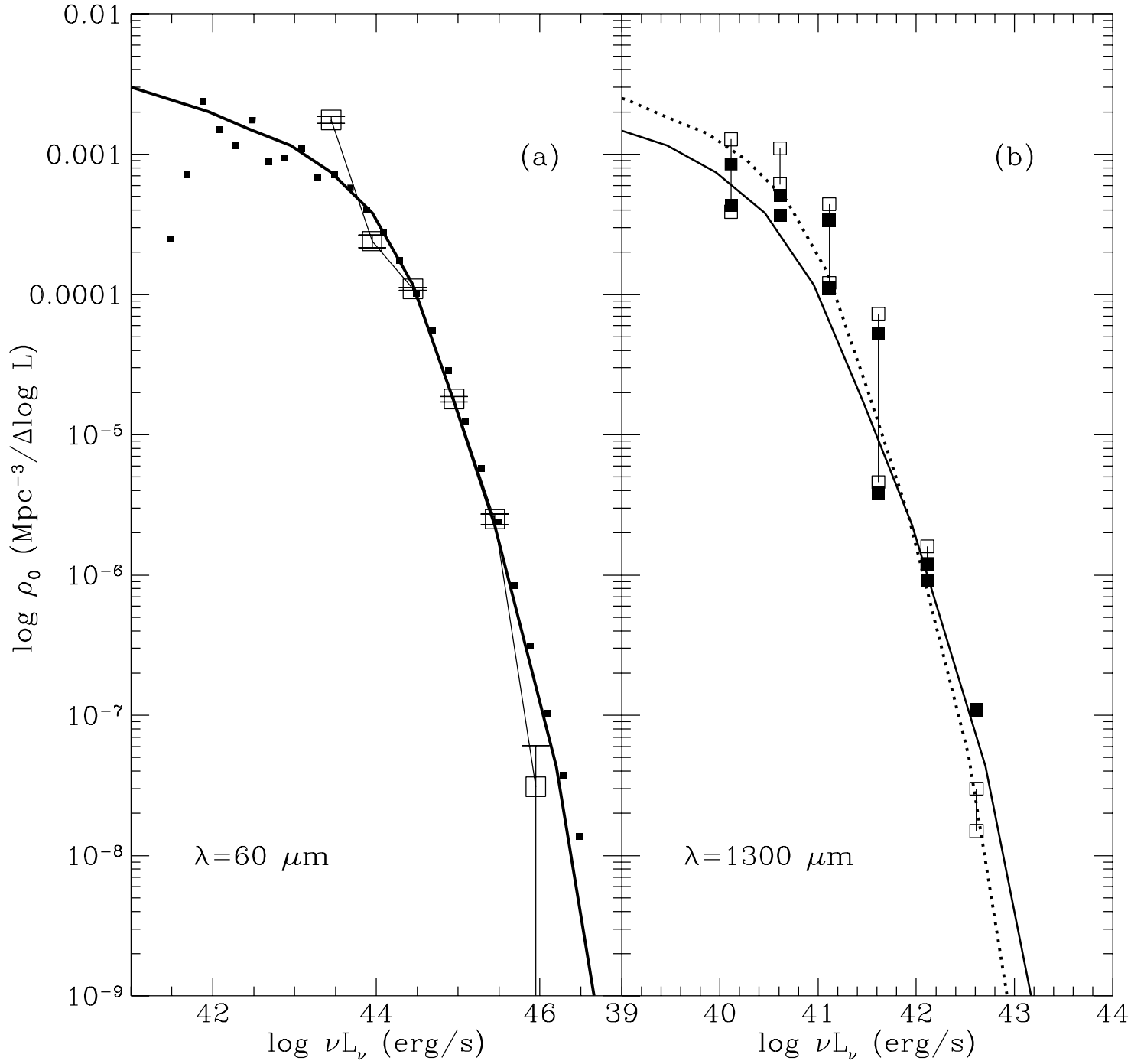
$\log L_{1.3mm}$ (erg/s/Hz)						
28.75	$2.7 \cdot 10^{-4}$	$6.4 \cdot 10^{-4}$	—	—	—	—
	$2.4 \cdot 10^{-4}$	$2.6 \cdot 10^{-4}$	—	—	—	—
29.25	$1.1 \cdot 10^{-3}$	—	—	—	—	—
	$0.27 \cdot 10^{-3}$	—	—	—	—	—
29.75	$2.70 \cdot 10^{-4}$	$3.21 \cdot 10^{-4}$	$1.13 \cdot 10^{-4}$	$1.67 \cdot 10^{-5}$	—	—
	$0.32 \cdot 10^{-4}$	$0.16 \cdot 10^{-4}$	$0.37 \cdot 10^{-4}$	$0.75 \cdot 10^{-5}$	—	—
30.25	—	—	$9.87 \cdot 10^{-5}$	$1.33 \cdot 10^{-5}$	$1.31 \cdot 10^{-6}$	—
	—	—	$0.26 \cdot 10^{-5}$	$0.07 \cdot 10^{-5}$	$1.0 \cdot 10^{-6}$	—
30.75	—	—	—	—	$2.62 \cdot 10^{-6}$	—
	—	—	—	—	$0.29 \cdot 10^{-6}$	—
31.25	—	—	—	—	—	$2.41 \cdot 10^{-7}$
	—	—	—	—	—	$6.30 \cdot 10^{-8}$

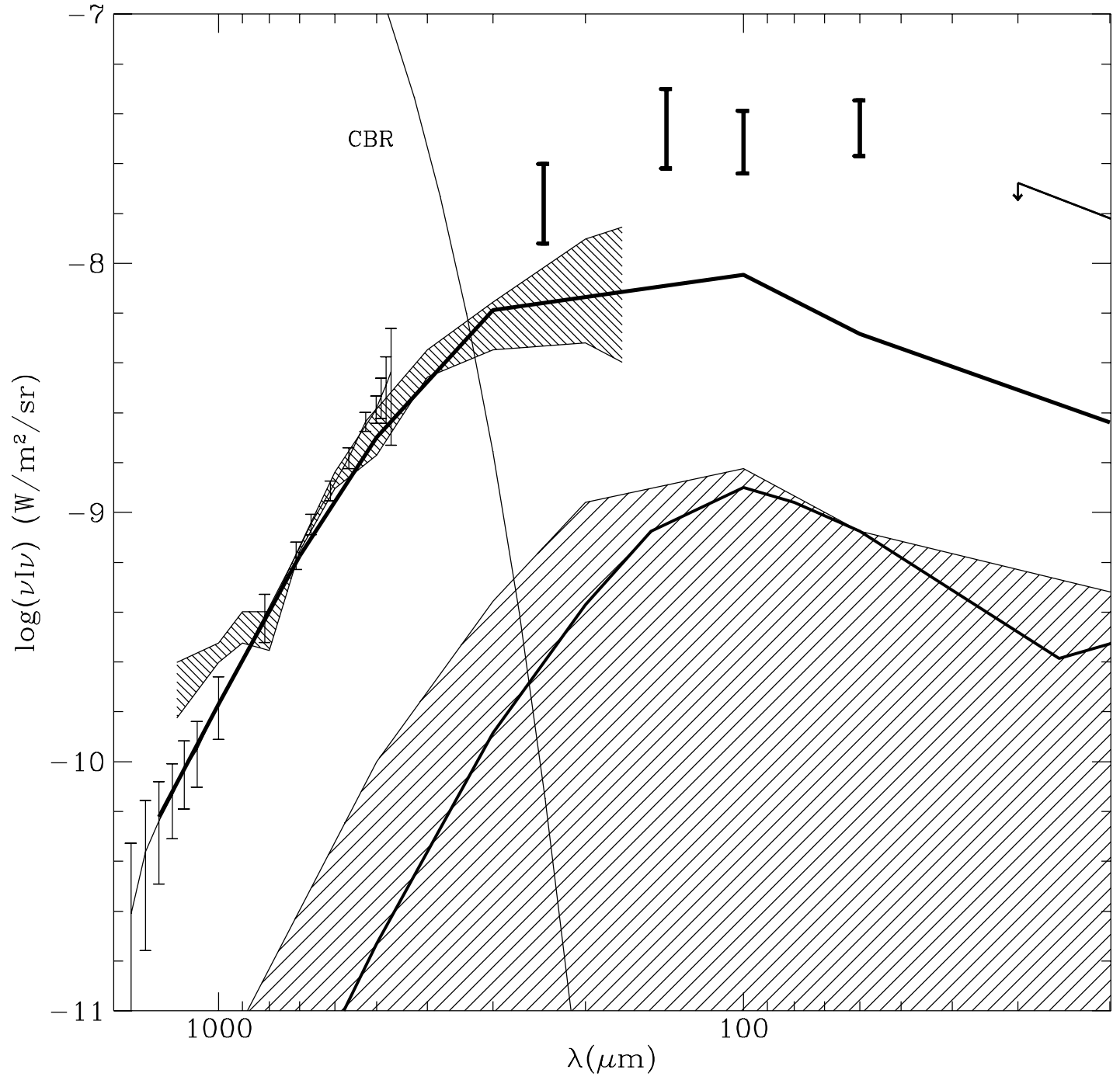
Table 2. Local Luminosity Function at 1.3mm

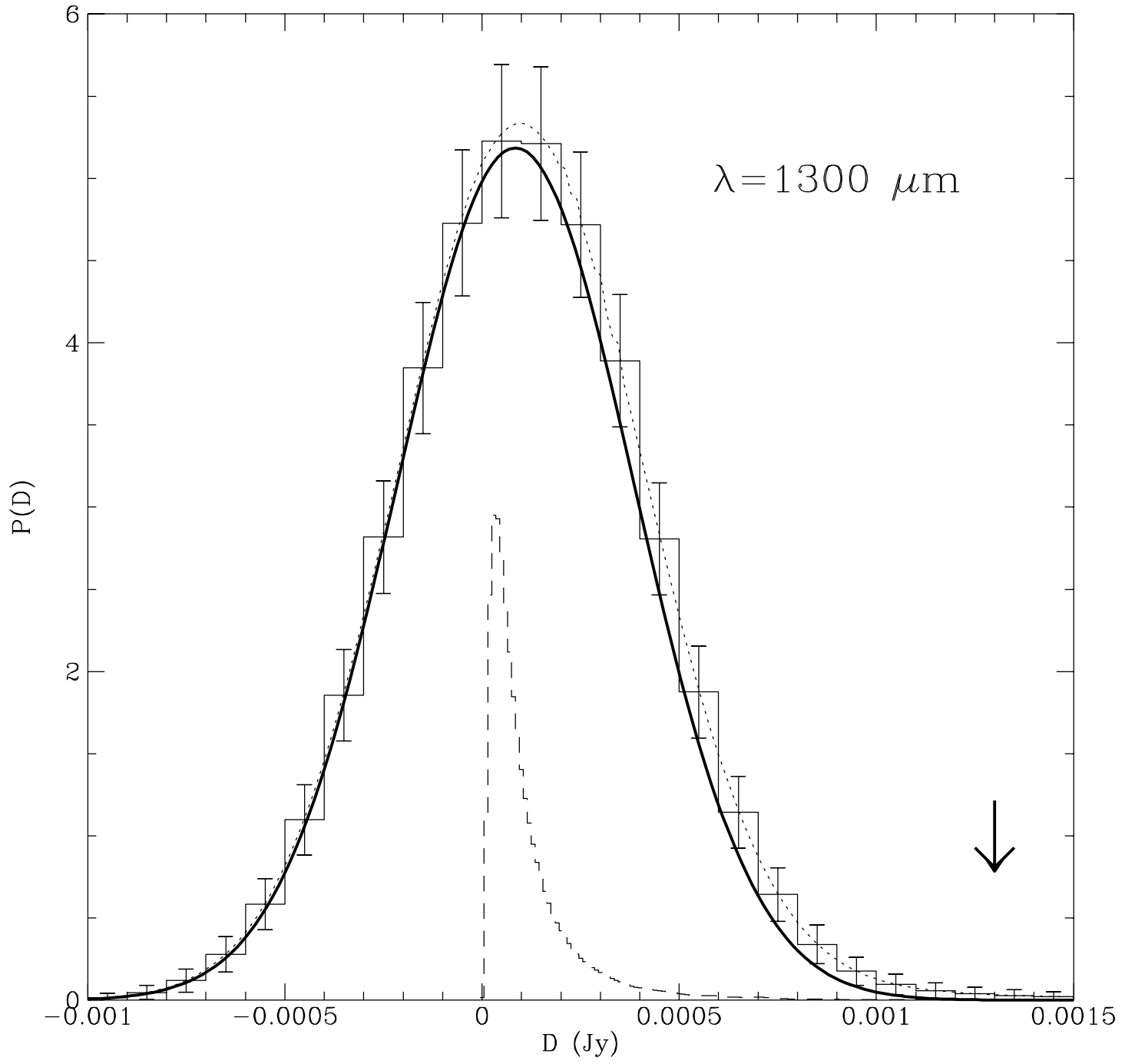
$\log L_{1.3mm}$ (erg/s/Hz)	$\log \rho_o$ ($Mpc^{-3} \Delta \log L_{1.3mm}$)	$\pm 2\sigma$
28.75	-3.1	0.13
29.25	-3.2	0.20
29.75	-3.7	0.20
30.25	-4.9	0.36
30.75	-5.9	0.15
31.25	-7.5	0.29

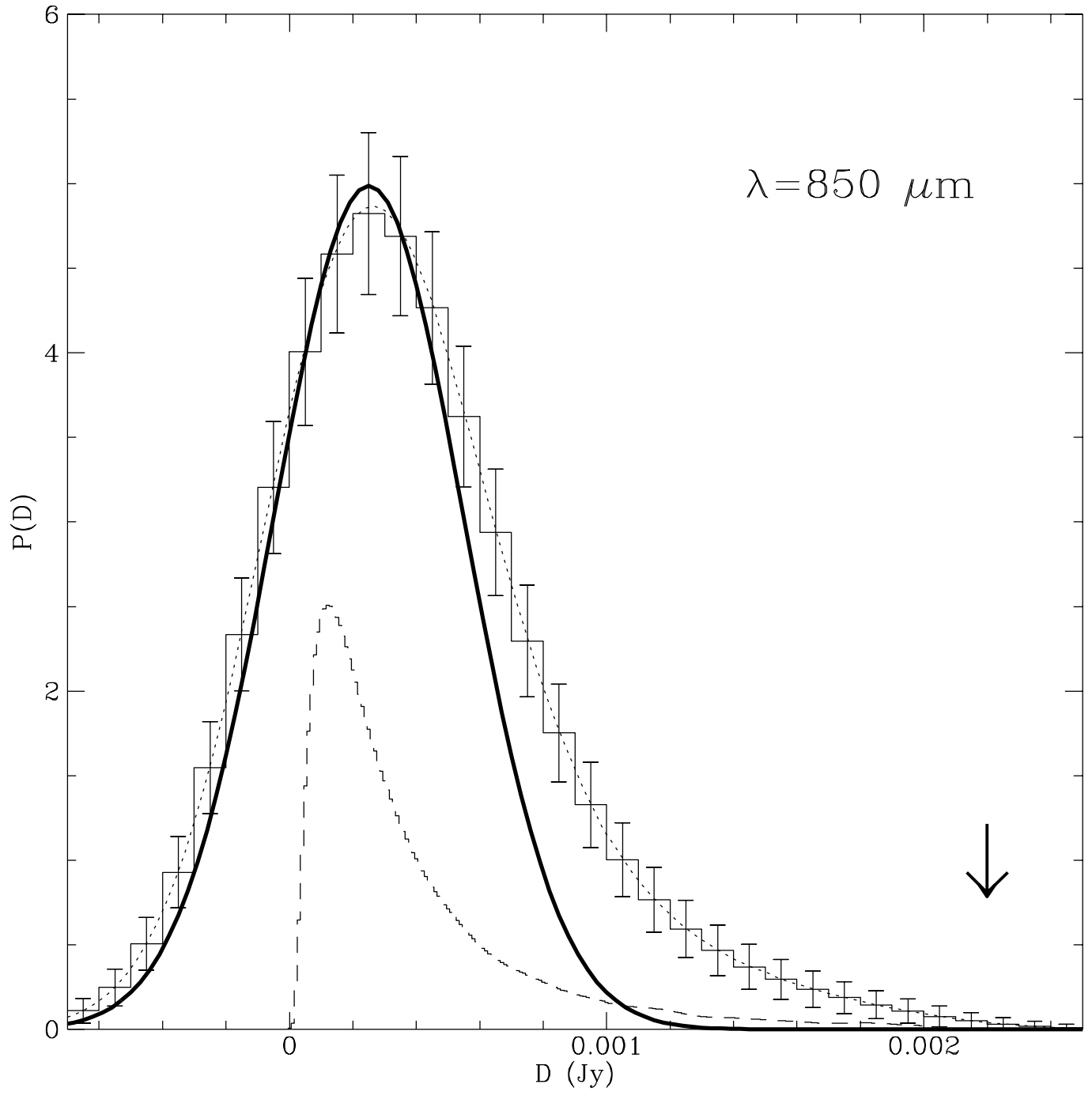












$\lambda = 850 \mu\text{m}$

